ISSN 1063-7842, Technical Physics, 2016, Vol. 61, No. 4, pp. 569–573. © Pleiades Publishing, Ltd., 2016.
Original Russian Text © A.A. Dedyukhin, P.N. Krylov, N.V. Kostenkov, R.M. Zakirova, I.V. Fedotova, 2016, published in Zhurnal Tekhnicheskoi Fiziki, 2016, Vol. 86, No. 4, pp. 91–95.

PHYSICS OF NANOSTRUCTURES

Effect of Thermal Annealing on the Structure of $ZnSe/Al_2O_3$ Nanocomposite Films

A. A. Dedyukhin, P. N. Krylov, N. V. Kostenkov, R. M. Zakirova, and I. V. Fedotova

Udmurt State University, Universitetskaya ul. 1, Izhevsk, 426034 Russia

e-mail: ftt@udsu.ru

Received July 13, 2015

Abstract—The $ZnSe/Al_2O_3$ nanocomposite films synthesized by laser evaporation followed by heat treatment are studied. X-ray diffraction and electron-microscopic investigations of the as-deposited films demonstrate the presence of ZnSe crystallites in an Al_2O_3 amorphous matrix. Annealing changes the structures of ZnSe and Al_2O_3, increases the ZnSe crystallite size, and causes the appearance of the $ZnSeO_4$ phase. The presence of aluminum oxide layers decreases the phase transformation temperature of zinc selenide.

DOI: 10.1134/S1063784216040095

INTRODUCTION

Owing to quantum-size effects, the nanocomposite structures containing nanocrystals of silicon, germanium, gallium arsenide, and cadmium or zinc sulfides and selenides in oxide matrices (Al_2O_3, SiO_x, GeO_x) have unique optical, photoluminescence, photoelectric, and catalytic properties [1–10], including a high selectivity and sensitivity to various gases [11]. The use of these nanocomposite structures with their high photo-, gas-, and thermosensitivity opens up fresh opportunities for designing combined sensitive elements for fire detectors for extremely early detection of fire sources and for ecological monitoring of atmosphere near hazardous plants and industrial centers and in thoroughfares.

The unique properties of low-dimensional materials and structures need new methods for their creation [12].

Pulsed laser deposition with various lasers for target ablation appeared in the late 1970s [13–16] and was widely used in flexible investigation techniques [12]. This method is universal for the material to be deposited. It makes it possible to exclude foreign impurities and to control the growth of film structures, which is very important for designing novel structures not produced by standard technologies [17, 18].

When considering the properties of nanocrystalline materials, researchers always take into account their metastability, which results from a high energy introduced in such materials. As compared to other well-known nonequilibrium metastable states, a nanocrystalline state has no equilibrium state that can correspond to it in structure and developed boundaries [19]. The following recrystallization processes occur in nanomaterials even at ordinary temperatures during a thermal action in force fields upon irradiation in the course of long-term operation: phase transformations, phase formation and decomposition, amorphization, sintering, and pore (nanocapillary) healing [20]. The sensor properties of composite films were improved after annealing [21]. The effect of temperature on the films grown under strongly nonequilibrium conditions modifies their properties [22]. It is often useful to perform additional heat treatment to stabilize the properties of nanomaterials [20].

The purpose of this work is to study the structure and the phase transformations in $ZnSe/Al_2O_3$ nanocomposite films formed by laser evaporation followed by heat treatment at various temperatures.

EXPERIMENTAL

$ZnSe/Al_2O_3$ nanocomposite films were synthesized by the formation of $ZnSe/Al_2O_3$ multilayer systems and their subsequent heat treatment.

As substrates, we used single-crystal KEF-4.5 silicon (100) wafers, fused KU-1 quartz plates, and cleaved NaCl single crystals. The silicon and quartz substrates were cleaned in a concentrated NaOH solution and then washed with distilled water. The cleanness of the substrate was estimated from the wettability of the substrate surface with water.

Film systems were grown by pulsed laser evaporation in an ultrahigh vacuum device [23]. The vacuum chamber was pumped out to $\sim 2 \times 10^{-5}$ Pa and was heated by an external heater to a temperature of 150°C for 4 h. To sputter ZnSe and Al_2O_3 targets, we used a CL-7100 excimer laser at a radiation wavelength $\lambda = 248$ nm, a pulse repetition frequency of 15 Hz, and a pulse duration of 20 ns. The substrate temperature during evaporation was maintained at a level of 20°C.

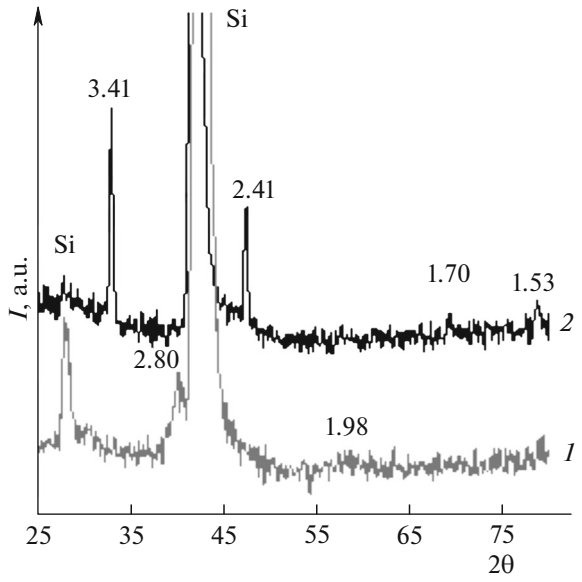

Fig. 1. X-ray diffraction patterns of $ZnSe/Al_2O_3$ films with 2-nm-thick ZnSe layers: (*1*) without annealing and (*2*) annealing at 800°C.

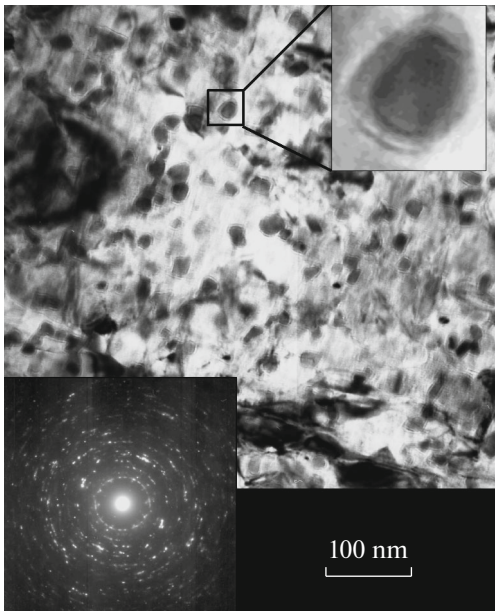

Fig. 2. TEM image and electron diffraction pattern of the $ZnSe/Al_2O_3$ system annealed at 800°C, magnification of ×100 000.

The first layer consisted of a 50-nm-thick Al_2O_3 film, and ZnSe (10 layers) then alternated with Al_2O_3 (9 layers). The ZnSe layer thickness was 4 nm and 2 nm, the Al_2O_3 layer thickness was 2 nm, and the thickness of the last upper Al_2O_3 layer was 5 nm. The total multilayer system thicknesses were 113 and 93 nm, respectively.

Under the same technological conditions, we also grew 170-nm-thick ZnSe films and 100-nm-thick Al_2O_3 films.

The grown multilayer $ZnSe/Al_2O_3$ systems were annealed in vacuum ($P \sim 2 \times 10^{-2}$ Pa) at temperatures of 600, 700, 800, 900, and 1000°C for 60 min.

X-ray diffraction (XRD) studies were performed on a computer-assisted DRON-3.0 diffractometer using FeK_α radiation in the Bragg angle range 30°–80° at a step of 0.1° and a recording time of 40 s per point.

Electron-microscopic analysis of the $ZnSe/Al_2O_3$ nanocomposite films was carried out on an EM-125 transmission electron microscope (TEM).

RESULTS AND DISCUSSION

As follows from XRD analysis of the as-deposited $ZnSe/Al_2O_3$ multilayer systems with a ZnSe layer thickness of 4 and 2 nm, zinc selenide is present in the cubic modification (two broad diffraction lines with interplanar spacings of 2.80 and 2.00 Å, JCPDS 37-1463) and aluminum oxide is amorphous. TEM data support the XRD results. The synthesized films are continuous. Their electron diffraction pattern corresponds to zinc selenide with a sphalerite structure, and the reflections corresponding to aluminum oxide are absent. Therefore, the synthesized system consists of zinc selenide and amorphous aluminum oxide crystallites.

Vacuum annealing of the $ZnSe/Al_2O_3$ films with a ZnSe layer thickness of 4 and 2 nm at a temperature of 600, 700, 800, 900, and 1000°C leads to the formation of zinc selenide crystallites of the hexagonal modification (interplanar spacings of 3.41, 2.41, 1.70, and 153 Å, JCPDS 15-105). As the annealing temperature increases, the diffraction lines corresponding to hexagonal zinc selenide become narrower, which indicates the coarsening of crystallites. No cubic ZnSe is detected after annealing (Fig. 1). Grain growth from 10 nm (600°C) to 100–200 nm (900 and 1000°C, respectively) is detected (grain size was estimated by the random intercept method). Electron micrographs (taken at a magnification of ×100000) of the samples annealed in the temperature range 600–800°C exhibit aggregates having a shell 2–3 nm thick (Fig. 2). These aggregates have a spherical (average diameter of 10–20 nm) or elongated (rectangular) shape and a size of 10 × 20 nm. No aggregates covered with a shell are detected in the $ZnSe/Al_2O_3$ nanocomposite films annealed at 900 and 1000°C. Round small "grains" about 5 nm in diameter are observed on the grain surfaces in the films annealed at 900°C, and such grains are absent on the grain surfaces in the films annealed at 1000°C.

An analysis of the electron diffraction patterns of the annealed nanocomposite systems shows that zinc selenide has the hexagonal structure of wurtzite.

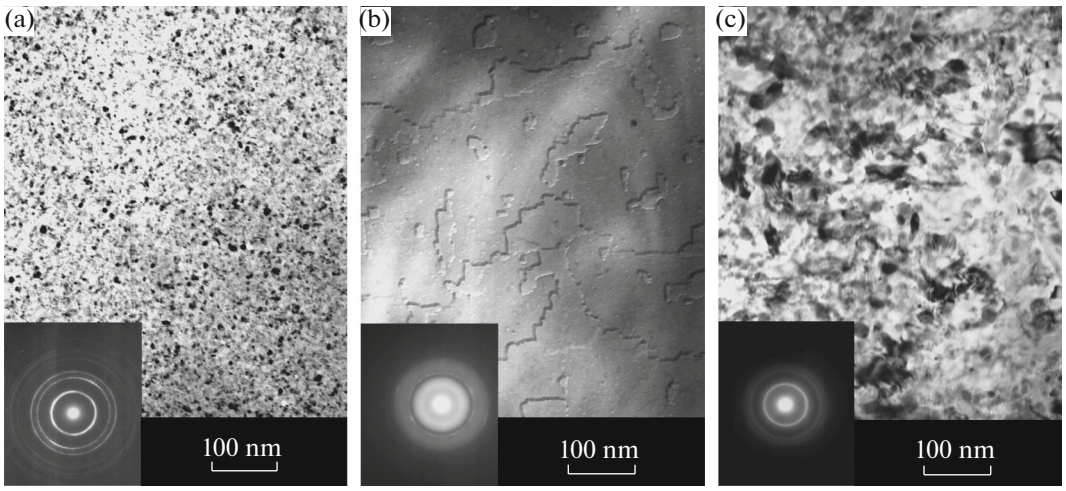

Fig. 3. TEM images and electron diffraction patterns of films: (a) ZnSe, (b) Al_2O_3, and (c) as-deposited $ZnSe/Al_2O_3$ system (4-nm-thick ZnSe layers).

Moreover, zinc selenate $ZnSeO_4$ appears upon annealing. Annealing at 800°C leads to the appearance of the cubic modification of Al_2O_3 (JCPDS 2-1421), and aluminum oxide at 900°C has the structure of corundum (α-Al_2O_3, JCPDS 42-1468). Electron diffraction patterns point to grain growth with increasing annealing temperature.

The as-deposited ZnSe films are polycrystalline and zinc selenide has the cubic modification of sphalerite (JCPDS 37-1463). The average grain size estimated by the random intercept method is 8.6 ± 0.6 nm (Fig. 3).

The Al_2O_3 film is homogeneous (Fig. 3), and its electron diffraction pattern contains two diffuse halos with point reflections. It should be noted that the film thickness is significantly larger than the layer thickness in the $ZnSe/Al_2O_3$ systems under study. According to [25], the crystallite size in films grown under the same conditions depends on the film thickness.

The phase transformation from sphalerite into wurtzite in zinc selenide occurs at 1698 K (1425°C) [26]. This transformation took place at a lower temperature upon vacuum annealing of the $ZnSe/Al_2O_3$ films. These results correlate with the data from [25, 26]. According to [27], ZnSe has the structure of sphalerite (cubic ZnS) in the $ZnSe/SiO_2$ composite thin films grown by the sol–gel method at a temperature of 500°C. The nanowires of thermally deposited zinc selenide and coated with microwave sputtered SiO_2 and the ZnSe nanowires coated with SiO_2 and annealed at 600°C in an O_2 or $N_2 + H_2$ atmosphere had a hexagonal structure [28].

The changes in the structure of the Al_2O_3 layers upon annealing of the $ZnSe/Al_2O_3$ nanocomposite films agree with the reported data on changes in the structure of Al_2O_3 films.

Corundum α-Al_2O_3 and defect-type γ-Al_2O_3 spinel are the most widespread and stable phases [29–31]. These phases can transform into each other, and this transformation depends on the method of sample synthesis, the presence of foreign atoms (impurities) in a lattice and/or chemical catalysts, and an external action [29, 30]. The results of studying the structures of Al_2O_3 films grown by various methods in vacuum are presented in [32–43]. The data on the γ-$Al_2O_3 \rightarrow$ α-Al_2O_3 phase transformations are conflicting [34–36].

The authors of [36, 37, 39–42] detected the formation of an amorphous aluminum oxide in the temperature range $T_s \sim 150$–350°C for various deposition methods. Ultrathin amorphous aluminum oxide films with nucleating α-Al_2O_3 crystallites were studied in [33].

As was shown in [33, 38], a fine columnar (fibrous) structure forms at a deposition temperature $T_s \sim 350$–400°C and is retained up to $T_s \sim 800$°C. As temperature T_s increases, clear diffraction lines corresponding to a phase with an fcc spinel structure and a lattice parameter that is close to that of γ-Al_2O_3 appear against the background of an amorphous (as determined by X-ray diffraction) phase. At $T_s = 800$°C, X-ray diffraction patterns have a diffuse halo at low angles ($2\theta = 5°$–30°), which points to the existence of an amorphous component. The X-ray diffraction patterns of samples thicker than 20 μm recorded at the same temperature contain weak lines of α-Al_2O_3. At $T_s \sim 940$°C, the formation of multiphase condensates consisting of a mixture of the γ and α phases at various α-phase contents was detected by an electron diffraction investigation. A more comprehensive study showed that the first signs of changing the phase composition (appearance of pronounced reflections of the thermodynamically stable α modification of Al_2O_3 in electron diffraction patterns) take place at $T_s \sim 825$°C.

Vacuum annealing at 900°C for 1 h of the Al_2O_3 condensates grown in the low-temperature range leads to the recrystallization of an amorphous matrix and the appearance of polycrystalline γ-Al_2O_3 [33]. It was assumed that the α phase could not form because of a too low annealing temperature or a too short annealing time for the γ-$Al_2O_3 \rightarrow \alpha$-$Al_2O_3$ phase transformation.

The temperature range of the $\gamma \rightarrow \alpha$ phase transformation is 700–1000°C for various methods of film deposition and various condensate thicknesses [33, 40, 43–45]. The amorphous Al_2O_3 layers in the $ZnSe/Al_2O_3$ nanocomposite films undergo such phase transformations upon annealing.

The appearance of $ZnSeO_4$ is likely to be related to the fact that the aluminum oxide deposited onto a substrate heated to 350–400°C has a spongy surface with a well developed network of channels and pores, and the corresponding films have defects [33]. Note a wide application of the low-temperature modifications of aluminum oxide, in particular, γ-Al_2O_3, in the catalyst industry [45]. We can also assume partial zinc reduction of aluminum upon annealing due to the high oxidation affinity of zinc.

CONCLUSIONS

The formation of $ZnSe/Al_2O_3$ nanocomposite films during laser evaporation followed by heat treatment at 600, 700, 800, 900, and 1000°C for 60 min was studied. The films consist of a 50-nm-thick Al_2O_3 sublayer, alternating ZnSe layers (10 layers) 4 and 2 nm thick and Al_2O_3 layers 2 nm thick, and an upper 5-nm-thick Al_2O_3 layer. The total multilayer system thicknesses were 113 and 93 nm, respectively.

TEM images of the as-deposited $ZnSe/Al_2O_3$ systems showed that they were continuous. Annealing was found to change the structure of ZnSe, to increase the crystallite size, to change the structure of Al_2O_3, and to result in the appearance of $ZnSeO_4$. The presence of aluminum oxide layers decreases the temperature of the phase transformation in zinc selenide.

The changes in the structure of the Al_2O_3 and ZnSe layers upon annealing of $ZnSe/Al_2O_3$ nanocomposite films agree with the reported data on changing the structure of Al_2O_3 films grown by various methods in vacuum and with the phase transformations in zinc selenide. We failed to find a discussion of the appearance of $ZnSeO_4$ in the $ZnSe/Al_2O_3$ system.

ACKNOWLEDGMENTS

This work was supported by the Ministry of Education and Science of the Russian Federation in terms of federal program Research and Development in the Priority Fields of the Scientific–Technological Complex in Russia in 2014–2020, project no. RFMEFI57414X0038.

REFERENCES

1. S. I. Pokutnii, Semiconductors **47**, 791 (2013).
2. Y. Kanemitsu, Phys. Rep. **263**, 1 (1995).
3. A. G. Cullis, L. T. Canham, and P. D. J. Calcott, J. Appl. Phys. **82**, 909 (1997).
4. D. Kovalev, H. Heckler, G. Polisski, and F. Koch, Phys. Status Solidi B **215**, 871 (1999).
5. O. Bisi, S. Ossicini, and L. Pavesi, Surf. Sci. Rep. **38**, 1 (2000).
6. Yu. V. Kryuchenko and A. V. Sachenko, Phys. E **14**, 299 (2002).
7. N. Kouklin, L. Menon, A. Z. Wong, D. W. Thompson, J. A. Woollam, P. F. Williams, and S. Bandypadhyay, Appl. Phys. Lett. **79**, 4423 (2001).
8. I. P. Lisovskii, S. A. Zlobin, E. B. Kaganovich, E. G. Manoilov, and E. V. Begun, Semiconductors **42**, 560 (2008).
9. A. A. Dedyukhin, R. M. Zakirova, N. V. Kostenkov, P. N. Krylov, and I. V. Fedotova, Vak. Tekh. Tekhnol. **19** (1), 33 (2009).
10. V. M. Vetoshkin, A. A. Dedyukhin, P. N. Dedyukhin, and I. V. Fedotova, Khim. Fiz. Mezoskopiya **11**, 223 (2009).
11. *Nanotechnology Research Directions: IWGN Workshop Report: Vision for Nanotechnology in the Next Decade,* Ed. by M. K. Roco, R. S. Williams, and P. Alivisatos (Kluwer, Dordrecht, 2000).
12. O. A. Novodvorskii, "Pulse laser depositions of thin films and nanosize structures for laser active media," Candidate's Dissertation in Physics (Shatura, 2012).
13. Z. P. Beketova, S. V. Gaponov, B. S. Kaverin, B. A. Nesterov, and N. N. Salashchenko, Izv. Vyssh. Uchebn. Zaved., Radiofiz. **18**, 908 (1975).
14. S. V. Gaponov, B. M. Luskin, B. A. Nesterov, and N. N. Salashchenko, Pis'ma Zh. Tekh. Fiz. **3**, 573 (1977).
15. S. V. Gaponov, B. M. Luskin, and N. N. Salashchenko, Tech. Phys. Lett. **5**, 210 (1979).
16. D. Lubben, S. A. Barnett, K. Suzuki, S. Gorbatkin, and J. E. Greene, J. Vac. Sci. Technol. B **3**, 968 (1985).
17. E. N. Sobol', A. P. Sviridov, V. N. Bagratashvili, V. N. Burimov, and V. N. Okorokov, Sverkhprovodimost: Fiz., Khim., Tekh. **5** (1), 128 (1992).
18. O. V. Boyarkin, V. N. Burimoe, V. S. Golubev, A. N. Zherikhin, and V. L. Popkov, Izv. Ross. Akad. Nauk, Ser. Fiz. **52** (12), 90 (1993).
19. V. S. Zhigalov, "Special features of the structure, phase states and magnetic properties of nanocomposite films of 3d metals produced by ultrafast condensation," Candidate's Dissertation in Physics (Krasnoyarsk, 2003).
20. R. A. Andrievskii, Usp. Khim. **71**, 967 (2002).
21. O. M. Stukalov, A. V. Misevich, A. E. Pochtennyi, M. O. Gallyamov, and I. V. Yaminskii, Poverkhnost, No. 11, 94 (2000).
22. A. I. Bazhen, A. E. Pokintelitsa, N. S. Shcheglova, V. A. Stupak, and A. N. Trotsan, Aktual. Probl.

Fizikokhim. Materialoznavstva, No. **4** (102), 109 (2013).

23. A. A. Dedyukhin, P. N. Krylov, and I. V. Fedotova, Vak. Tekh. Tekhnol. **20** (1), 9 (2010).
24. C. S. Alalykin and P. N. Krylov, Prib. Tekh. Eksp., No. 2, 149 (2005).
25. G. Hass and, R. E. Thun, *Physics of Thin Films* (Academic, New York, 1966), Vol. 3.
26. M. P. Kulakov, V. D. Kulakovskii, I. B. Savchenko, and A. V. Fadeev, Sov. Phys. Solid State **18**, 526 (1976).
27. H.-Q. Jiang, X. Yao, J. Che, X. Wan, and M.-Q. Wang, J. Electroceram., No. 21, 733 (2008).
28. H. Kim, C. Jin, S. An, and C. Lee, Bull. Korean Chem. Soc. **33**, 398 (2012).
29. N. A. Toropov, V. P. Barzakovskii, I. A. Bondar', and Yu. P. Udalov, *Phase Diagrams of Silicate Systems* (Nauka, Leningrad, 1970).
30. I. P. Batra, J. Phys. C **15**, 5399 (1982).
31. D. A. Zatsepin, V. R. Galakhov, B. A. Gizhevskii, E. Z. Kurmaev, V. V. Fedorenko, A. A. Samokhvalov, and S. V. Naumov, Phys. Rev. B **59**, 211 (1999).
32. D. A. Zatsepin, V. M. Cherkashenko, E. Z. Kurmaev, S. N. Shamin, V. V. Fedorenko, N. A. Skorikov, S. V. Plastinin, N. V. Gavrilov, A. I. Medvedev, and S. O. Cholakh, Phys. Solid State **46**, 2134 (2004).
33. P. V. Seredin, D. L. Goloshchapov, A. N. Lukin, A. S. Len'shin, A. D. Bondarev, I. N. Arsent'ev, L. S. Vavilova, and I. S. Tarasov, Semiconductors **48**, 1527 (2014).
34. H. C. Lin, P. D. Ye, and G. D. Wilk, Appl. Phys. Lett. **87**, 182 904 (2005).
35. Y. Xuan, Y. Q. Wu, H. C. Lin, T. Shen, and D. Ye. Peide, IEEE Electron Device Lett. **28**, 935 (2007).
36. T. C. Chou, T. G. Nieh, S. D. McAdams, and G. M. Pharr, Scr. Metall. **25**, 2203 (1991).
37. A. L. Borisova, D. I. Adeeva, and V. N. Sladkova, Avtom. Svarka, No. **9** (534), 26 (1997).
38. L. A. Krushinskaya and Ya. A. Stel'makh, Vopr. At. Nauki Tekh., Ser.: Vak., Chist. Mater., Sverkhprovodn. **19** (6), 92 (2011).
39. G. Hoetzsch, O. Zywitzki, and H. Sahm, in *Proceedings of the 40th Annual Technical Conference of the Society of Vacuum Coaters, New Orlean, 1997*, p. 77.
40. I. V. Lunev and V. G. Padalka, Metallofiz. Noveishie Tekhnol. **22** (2), 36 (2000).
41. K. A. Osipov, T. L. Borovich, and I. I. Orlov, Neorg. mater. **7**, 1970 (1971).
42. *Encyclopedia of Nonorganic Materials* (Ukr. Sov. Entsiklopediya, Kiev, 1977), Vol. 2.
43. B. A. Movchan and T. A. Molodkina, Fiz. Khim. Obrab. Mater., No. 3, 107 (1978).
44. N. E. Strucheva, V. D. Kartavykh, and V. A. Novozhenov, Izv. Altai. Gos. Univ., No. 3–2, 177 (2010).
45. V. Sh. Bakhtadze, V. P. Mosidze, D. G. Kartvelishvili, R. V. Dzhandzhgava, and N. D. Kharabadze, Katal. Prom-sti., No. 2, 56 (2012).

Translated by K. Shakhlevich